Eur. Phys. J. E (2011) **34**: 136
DOI 10.1140/epje/i2011-11136-2

THE EUROPEAN PHYSICAL JOURNAL E

Regular Article

Dynamics of semi-flexible tethered sheets

A simulation study using stochastic rotation dynamics

S.B. Babu[a] and H. Stark

Institut für Theoretische Physik, Technische Universität Berlin, Hardenbergstraße 36, D-10623 Berlin, Germany

Received 14 June 2011 and Received in final form 21 October 2011
Published online: 28 December 2011 – © EDP Sciences / Società Italiana di Fisica / Springer-Verlag 2011

Abstract. The dynamics of a semi-flexible sheet or tethered membrane in a solvent is studied using the method of stochastic rotation dynamics. Hydrodynamic interactions between different parts of the sheet are naturally included in this method. We confirm the scaling law for the radius of gyration *versus* sheet size predicted for a self-avoiding tethered membrane. The mean-square displacement shows both sub-diffusive and diffusive behavior similar to linear polymers. In the intermediate scattering function the sub-diffusive behavior appears as stretched exponential which we reproduce in our simulations. Thereby, we confirm an early prediction between the roughness and the sub-diffusion exponent derived from Zimm dynamics (E. Frey, D.R. Nelson, J. Phys. I **1**, 1715 (1991)). Finally, we show that the diffusion coefficient of the square sheet is inversely proportional to the edge length of the sheet again in good agreement with theoretical predictions.

1 Introduction

The study of soft matter systems like polymers [1] leads to a thorough understanding of the structural and dynamic properties of this rather complex material system. For example, to describe the diffusion of linear polymers, two models based on bead-spring chains are used: the Rouse model, which only employs local friction coefficients of the beads [2], and the Zimm model, which also includes hydrodynamic interactions between them [3]. Tethered membranes [4], which can be considered the two-dimensional analog of a polymer, have also attracted considerable interest because they occur in a variety of real system like red blood cells [5] or graphite oxide sheets [6]. Although the structure of membranes has received much attention [4, 7, 8], very few studies have concentrated on their dynamics [9–12].

In this paper we study a two-dimensional model system that we call a tethered sheet in analogy to tethered membranes. We model the sheet with beads connected by springs so that each bead has fixed connectivity. The sheet, therefore, represents a polymerized membrane rather than a fluid membrane where the connectivity between nearest neighbors is not fixed [4]. In general, such sheets exhibit a wide range of conformational changes like wrinkles and crumpling under different external condition such as temperature, quality of solvent, etc. [7, 8]. Here, we introduce additional bending rigidity along the sheet, so in equilibrium it is flat. However, as the rigidity of the sheet is decreased or the temperature of the solvent is increased, the sheet will undergo a phase transition from a flat to a crumpled configuration [4]. In this paper, we study the diffusion of a flat sheet under a range of external parameters such as varying size, viscosity, etc. Because of the highly constrained motion of the vertices of the sheet, diffusion becomes non-trivial. Recently, there has been renewed interest in simulating the dynamics of such sheets using Monte Carlo simulations [11–13]. In particular, these studies could not consider the influence of hydrodynamic interactions between the vertices of the sheet.

A variety of numerical methods exists to simulate low Reynolds number hydrodynamics. The method of mobilities, which includes the solvent implicitely, is an effective and simple method to implement hydrodynamic interactions between spherical constituents [14]. A drawback of this method is the difficulty to treat complex geometries such as a sheet. In this work, in order to simulate hydrodynamics interactions between the vertices of the sheet, we use stochastic rotation dynamics (SRD) also known as multi-particle collision dynamics [15–17]. SRD introduces coarse-grained solvent particles, describes their dynamics with the help of ballistic and collision steps, and thereby is able to generate solutions of the Navier-Stokes equations [15,16]. SRD has been employed to study dynamical properties in a variety of systems like polymers [18], colloids [19], biological system [20, 21] etc., just to name a few. As this technique includes thermal fluctuation, it is the method of our choice.

Even though the structure of elastic sheets has extensively been investigated [4, 7, 8], very few studies have

[a] e-mail: sujin_bb@yahoo.co.in

treated diffusion of a sheet where hydrodynamic interactions are explicitly taken into account [9,10]. In this paper we address the problem in detail by simulating the dynamics of a tethered sheet with bending rigidity using the method of stochastic rotation dynamics. We address the mean-square displacement and the intermediate scattering function of the sheet and demonstrate that their behavior is similar to a single polymer. In particular, we confirm that the diffusion of an isolated sheet can also be explained by Zimm dynamics as in polymeric systems. Our results agree well with previous predictions and show that stochastic rotation dynamics is able to simulate the properties of tethered sheets.

In sect. 2 we introduce our model and explain how we implement the interaction of the sheet with the SRD solvent. In sect. 3 the results of our simulations are discussed followed by a conclusion in sect. 4.

2 Model

2.1 Modeling a tethered sheet

In this work we always consider a square sheet in a three-dimensional environment. The sheet is made of vertices that are distributed on a lattice as shown in fig. 1(a). Neighboring vertices are connected by Hookean springs. In order to provide the sheet with some in-plane shear resistance, we also connect next-nearest neighbor vertices with Hookean springs. The potential for the harmonic spring force is given by

$$\frac{U_s}{k_BT} = \frac{1}{2l_0^2}\kappa_s(l-l_0)^2, \tag{1}$$

where κ_s is the spring constant, k_BT is the thermal energy, and l_0 is the equilibrium length of the springs. In order to prevent the sheet from crumbling, we apply a bending potential along the two main directions of the sheet

$$\frac{U_b}{k_BT} = \kappa_b(1-\cos\theta). \tag{2}$$

Here κ_b is the bending stiffness and θ is the angle between the two bond vectors that point from one vertex to its two nearest neighbors along one main direction of the sheet [14]. In this work we choose $\kappa_s = 100$ and $\kappa_b = 100$. Since a transition to a crumpled sheet would take place at $\kappa_b < 30$ [22], we are only dealing with a flat sheet. The number of vertices in the sheet is $N = (L+1)^2$, where L is the edge length of the sheet in units of the equilibrium distance of nearest-neighbor vertices. The velocities and positions of the vertices with mass $m = 1$ are always given in dimensionless units. They are updated during a molecular dynamics (MD) step by the velocity Verlet algorithm using the time step δt_{MD} [23]

$$\mathbf{r}_i(t+\delta t_{\mathrm{MD}}) = \mathbf{r}_i(t) + \delta t_{\mathrm{MD}}\mathbf{v}_i(t) + \frac{1}{2}\delta t_{\mathrm{MD}}^2\frac{\mathbf{F}_i(t)}{m}, \tag{3}$$

$$\mathbf{v}_i(t+\delta t_{\mathrm{MD}}) = \mathbf{v}_i(t) + \frac{1}{2}\delta t_{\mathrm{MD}}\left[\frac{\mathbf{F}_i(t)}{m} + \frac{\mathbf{F}_i(t+\delta t_{\mathrm{MD}})}{m}\right]. \tag{4}$$

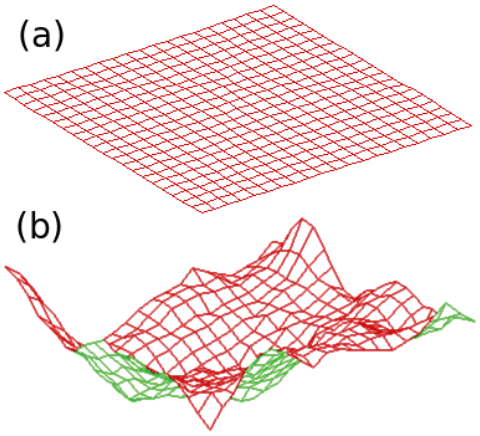

Fig. 1. Snapshot of a sheet with edge lenght $L = 20$ (in units of the distance of nearest-neighbor vertices). (a) Initial configuration, (b) after reaching thermal equilibrium in the simulation. The hight fluctuations are scaled up by a factor of 6 to make them visible.

Here $\mathbf{r}_i$, $\mathbf{v}_i$ and $\mathbf{F}_i = -\nabla_i\frac{U_s+U_b}{k_BT}$ are the respective position, velocity, and force of the i-th vertex of the sheet. To perform the gradient ∇_i of the spring and bending energy $U_s + U_b$ with respect to $\mathbf{r}_i$, the energies are discretized in the position variables $\mathbf{r}_i$. A typical snapshot of the sheet after reaching thermal equilibrium is shown in fig. 1(b). The height fluctuations are scaled up by a factor of 6, otherwise the sheet would look essentially flat.

2.2 Modeling the SRD fluid

In our SRD simulations, fictitious fluid particles (point particles) are introduced and distributed in a three-dimensional simulation box with periodic boundary conditions. We start with a thermally equilibrated system and assign each fluid particle a velocity from a three-dimensional Gaussian distribution with variance $3k_BT/m$. We choose units such that the mass m of the fluid particle and thermal energy k_BT are one. In SRD the fluid particles move according to a sequence of streaming and collision steps. In the streaming step the particles move ballistically during a time interval δt,

$$\mathbf{r}_i(t+\delta t) = \mathbf{r}_i(t) + \delta t\mathbf{v}_i(t)\ . \tag{5}$$

During the streaming step the fluid particles are not allowed to penetrate the sheet. For this reason we break the streaming step into p molecular dynamics step, such that $\delta t = p\delta t_{\mathrm{MD}}$. Throughout this work, we keep $\delta t_{\mathrm{MD}} = 10^{-3}$ and in most of the cases we choose δt close to 10^{-2}. If the fluid particle penetrates the sheet, it is moved back to the surface of the sheet and stochastically bounced back. This means that the new velocity of the fluid particle is generated according to the following rule. The velocity component v_n of the particle along the surface normal is taken from a Rayleigh distribution and the tangential

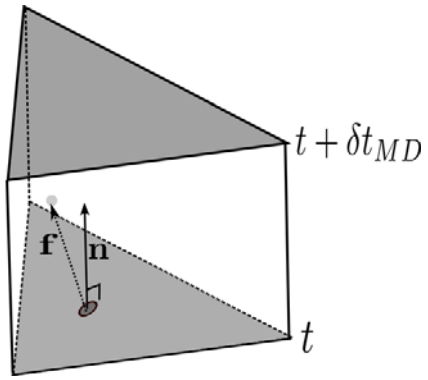

Fig. 2. Schematic representation for detecting solvent particles inside the volume defined by the same triangle at times t and $t + \delta t_{\rm MD}$. $\mathbf{n}$ is a unit vector normal to one face and $\mathbf{f}$ points from the center of area of this face to the solvent particle.

component v_t from a Gaussian distribution:

$$P(v_n) \propto v_n \exp(-mv_n^2/2k_BT), \quad (6)$$

$$P(v_t) \propto \exp(-mv_t^2/2k_BT). \quad (7)$$

After the collision the change in momentum of the fluid particle is added to the nearest vertex of the sheet so as to conserve the total momentum of the system. It has been shown that this method satisfies the no-slip boundary condition [24].

After the positions of the sheet have been moved in a MD step with time interval $\delta t_{\rm MD}$, one has to check if a solvent particle has passed through any part of the sheet. For this we use the triangulation of the sheet and determine if a solvent particle is inside the volume defined by the same triangle at times t and $t + \delta t_{\rm MD}$ (see fig. 2). For each face of the volume we calculate the inward normal $\mathbf{n}$ and the position vector $\mathbf{f}$ of the solvent particle relative to an arbitrary point on the face, *e.g.*, its center of area. If the projection of $\mathbf{f}$ on $\mathbf{n}$ is positive for all five faces ($\mathbf{f} \cdot \mathbf{n} > 0$), then the solvent particle has passed through the sheet. To avoid such an event for the whole sheet, we advance it by half the time step and repeat the analysis. This procedure is continued until the sheet does not cross any solvent particle. The solvent particles are then moved ballistically in the streaming step for the same amount of time. This procedure is repeated until the resulting sequence of streaming steps takes approximately the time δt.

After p MD steps we perform a collision step. For the collision step we divide the simulation box into cells of edge length a. In the present work we keep $a = 1$ and the average number of fluid particles per cell is $\rho = 5$. The simulation time is measured in units of $\sqrt{ma^2/k_BT}$ which is equal to one. In the collision step the relative velocity of each particle with respect to the center-of-mass velocity $\mathbf{V}_j$ of all fluid particles in cell j is determined and then rotated by a constant angle α about a random axis. Hence, after a collision the velocity of the i-th particle in the j-th cell is given by

$$\mathbf{v}_i(t + \delta t) = \mathbf{V}_j(t) + \mathbf{R}_j[\mathbf{v}_i(t) - \mathbf{V}_j(t)], \quad (8)$$

where $\mathbf{R}_j$ is the rotation matrix which rotates a vector by an angle α about a randomly chosen axis. In our simulation we always choose $\alpha = 2\pi/3$. The collision step transfers momentum between the particles in the cell but conserves the total momentum and energy of each cell. We do not conserve angular momentum during the collision step in SRD, as it is not relevant for the study of diffusional properties [18]. The vertices of the sheet are also included in the collision step which ensures no-slip boundary conditions during the collision step as suggested for polymers [18] and biological systems [25]. As the streaming time step is very small $\delta t \ll 1$, artificial correlations between particles of the same cell develop. We perform random shifts of the cells for each new collision step in order to preserve Galilean invariance as proposed in [26,27].

The sequence of streaming and collision steps is sufficient to generate a solution of the Navier-Stokes equation [15–17]. In addition, thermal fluctuations are naturally included in the method. Both collision and streaming step contribute to the viscosity of the SRD fluid, $\eta = \eta_{\rm cl} + \eta_{\rm st}$, for which analytical expressions exists [15–17]. In particular, viscosity is controlled by the time interval δt of the streaming step. For the rotation angle $\alpha = 2\pi/3$, we obtain for the contribution from the collision step, $\eta_{\rm cl} = 0.067/\delta t$, and for the streaming step, $\eta_{\rm st} = 0.54\delta t$. Unless otherwise stated in the text, most of the simulations are performed for $\delta t = 0.01$, *i.e.*, for a viscosity $\eta = 6.7$ which is mainly determined by the collision step. Since $\delta t \ll 1$, fluid particles stream a distance much smaller than the cell size between two collision steps. So, in our simulations, the collision step serves as the primary mechanism for transfering momentum between fluid particles and, therefore, determines the hydrodynamic interactions between the vertices of the sheet. The edge length of the cubic simulation box $L_{\rm box}$ ranges from 30 to 200 and the number of SRD fluid particles simulated is between 13.5×10^4 and 40×10^6.

3 Results and discussion

The structural properties of tethered membranes have extensively been studied as documented, *e.g.*, by refs. [4,7,8]. In the present work, we mainly concentrate on diffusional properties of the membrane. For this reason, we investigate the mean-square displacement of the sheet and also look at the intermediate scattering function to address its internal dynamics.

In fig. 3 we first plot the radius of gyration $\langle R_g^2 \rangle$ against the square of the edge length L^2 of the sheet. The radius of gyration is defined by

$$\langle R_g^2 \rangle = \frac{1}{N} \sum_{i=1}^{N} \langle (\mathbf{r}_i - \mathbf{r}_{\rm cm})^2 \rangle, \quad (9)$$

where $N = (L+1)^2$ is the total number of vertices, $\mathbf{r}_i$ is the position of the i-th vertex, and $\mathbf{r}_{\rm cm}$ is the center of mass of the sheet. According to Flory's scaling argument, one expects the scaling relation $\langle R_g^2 \rangle \propto L^{2\nu}$ if a two-dimensional

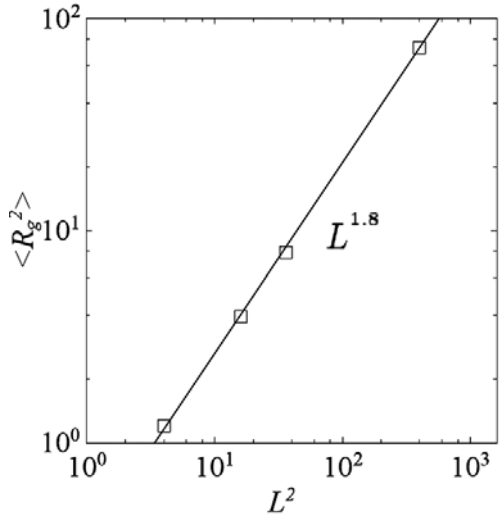

Fig. 3. The square of the radius of gyration is plotted against the square of the edge length L^2 of the sheet. The solid line represents the scaling relation, $R_g^2 \propto L^{2\nu}$, with exponent $\nu = 0.9$.

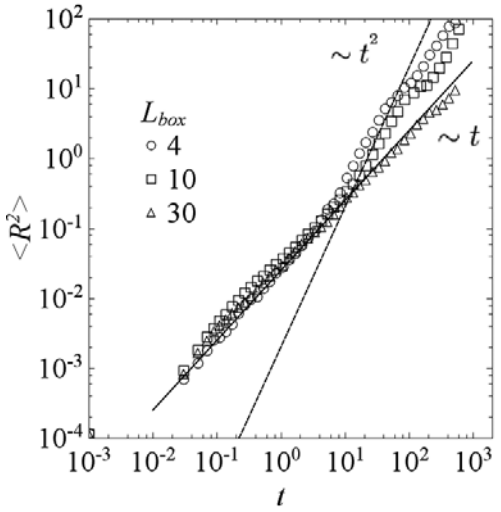

Fig. 4. The MSD is plotted as a function of time for a sheet with edge length $L = 2$ for different simulation box sizes given by the edge length $L_{\rm box}$ as indicated in the plot. The solid line has a slope of one and the dashed line a slope of two.

sheet is embedded in a three-dimensional environment [7]. For a crumbled sheet $\nu \approx 0.67$ [7] and for a flat sheet the upper bound $\nu = 1$ should occur [7, 11, 12]. Our results in fig. 3 are consistent with the scaling relation and give an exponent $\nu = 0.9$, which means that the sheet is essentially flat. The deviation from $\nu = 1$ is due to thermal fluctuations illustrated in fig. 1(b). For better visibility, they are scaled up by a factor of 6.

3.1 Mean-square displacement

We define the mean-square displacement (MSD) $\langle R^2 \rangle$ of the sheet by averaging over all vertices

$$\langle R^2 \rangle = \frac{1}{N} \sum_{i=1}^{N} \langle (\mathbf{r}_i(t) - \mathbf{r}_i(0))^2 \rangle \ . \tag{10}$$

In fig. 4 we show how the size of the simulation box influences the temporal evolution of $\langle R^2 \rangle$ for a sheet with edge length $L = 2$. As the dynamics is due to thermal fluctuations caused by the solvent, we expect the motion of the sheet to be purely diffusive in the limit of large times ($\langle R^2 \rangle \propto t$). Initially, all the curves in fig. 4 have a slope of one which means normal diffusion. However, for the box size $L_{\rm box} = 2L$, when the MSD reaches a value of 0.1, $\langle R^2 \rangle$ starts to deviate from the diffusive behavior and is clearly accelerated. For a larger box size with $L_{\rm box} = 5L$ the acceleration only occurs at $\langle R^2 \rangle = 0.25$. Finally, at $L_{\rm box} = 15L$ the sheet dynamics is purely diffusive during the complete simulation time. It reaches $\langle R^2 \rangle = 10$ meaning that the sheet with edge length $L = 2$ has moved approximately 1.5 times its size. The reason for the dependence on the simulation box size $L_{\rm box}$ is that the sheet experiences hydrodynamic interactions with its images created by the implemented periodic boundary conditions. This is supported by the following consideration. A disturbance caused by the moving sheet spreads by vorticity diffusion and needs a time $t_h = L_{\rm box}^2/(2\eta/\rho)$ to diffuse a distance $L_{\rm box}$. With the dynamic viscosity $\eta/\rho = 6.7/5 = 1.34$ we find $t_h = 6$ for $L_{\rm box} = 4$ and $t_h = 37$ for $L_{\rm box} = 10$. This fits nicely to the time when the mean-square displacement in fig. 4 deviates from diffusive motion. Obviously, the flow fields from the images accelerate the sheet to a superdiffusive motion. As shown in fig. 4, when $L_{\rm box}$ is sufficiently large, finite-size effects are insignificant and do not influence the motion of the sheet since the strength of the diffusing vortex decays as $1/L_{\rm box}$. In the current work we always kept $L_{\rm box}$ 15 times the length of the sheet except for $L = 20$ where the simulation box size was 200.

As we are modeling a two-dimensional sheet, it is interesting to study whether the impenetrability of the sheet to the fluid particles is essential for the dynamics of the system. In fig. 5 we, therefore, compare the MSD of an impenetrable sheet and a penetrable sheet, where we allow the fluid particles to pass through the sheet during the streaming step. For a sheet of size $L = 4$, we do not see any appreciable difference in the MSD for both simulated cases. As already discussed in subsect. 2.2, the fluid particles stream for a very small distance between two collision steps as the duration of the streaming step is very small ($\delta t \ll 1$). So, transfer of momentum between the fluid particles and the sheet comes mainly from the collision step, which determines the viscosity of the fluid, $\eta \approx \eta_{\rm cl} = 0.067/\delta t$. This explains the result of fig. 5. Hence, for large sheets ($L = 20$) we let the fluid particles simply pass through the sheet, as the detection of particles that penetrate the sheet is the most time consuming part in our simulation.

In fig. 6 we plot the MSD for sheets of different sizes. The vertices of a sheet start to diffuse at very short times as shown in the inset of fig. 6 for size $L = 20$. When the

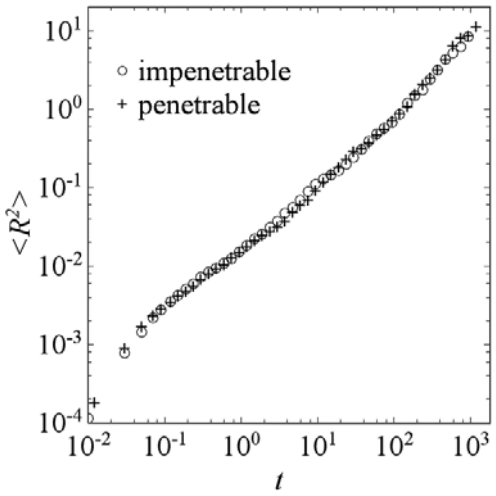

Fig. 5. The MSD is plotted as a function of time for a sheet with edge length $L = 4$, for an impenetrable sheet and a penetrable sheet, where the fluid particles are allowed to flow through the sheet, as indicated in the figure.

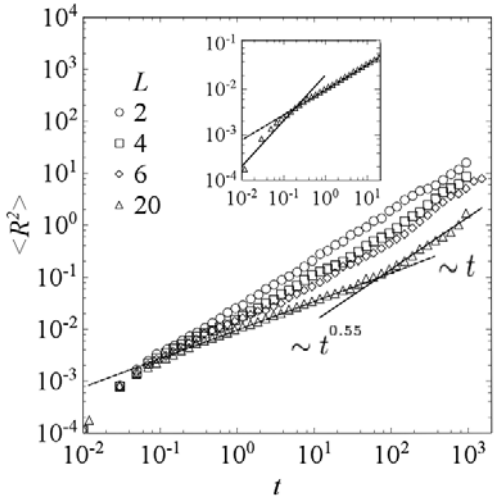

Fig. 6. The MSD is plotted *versus* time for sheets of different edge lengths L as indicated in the figure. The inset shows the MSD of the sheet with $L = 20$ at short times. In both graphs, the solid line has a slope of one and the dashed line has a slope of 0.55.

vertices experience the constraints due to the fixed connectivity, the sheet enters a sub-diffusive regime ($\langle R^2\rangle \propto t^\gamma$ with $\gamma < 1$) which is most pronounced for the largest sheet as indicated by the dashed line in fig. 6. Finally, all sheets enter the expected diffusive regime for large times. This behavior is similarly observed for linear polymers where the individual motion of a monomer is hindered by the presence of bonds to its neighbors. Whereas the Rouse model [2], which neglects hydrodynamic interactions between monomers, gives $\langle R^2\rangle \propto t^{1/2}$ for the sub-diffusive dynamics, the Zimm model results in $\langle R^2\rangle \propto t^{2/3}$ by taking into account hydrodynamic interactions [3].

Monte Carlo simulations for a flat membrane implement the Rouse model and suggest the scaling relation $\langle R^2\rangle \propto t^{0.3}$ [12]. Our simulations instead correspond to the Zimm model. For the largest sheet we find $\langle R^2\rangle \propto t^{0.55}$ (dashed line in fig. 6). Therefore, in analogy to linear polymers, the value of γ is higher in our Zimm-like compared to the Rouse-like simulations in [12]. Also, the value $\gamma = 0.55$ observed for our largest sheet is smaller than the exponent 2/3 for linear polymers. This makes sense since vertices in a sheet are more constrained due to the increased connectivity.

As we increase the size of the sheet, its radius of gyration also increases which progressively slows down the diffusion of the sheet. In addition, the sub-diffusive regime in fig. 6 is more pronounced for larger sheets. We give a qualitative explanation for this observation. For constant bending rigidity the flexibility and, as we discuss below, the fluctuations of the sheet increase with its size. A small sheet behaves basically as a rigid object. The sub-diffusive regime is due to the internal motion of the vertices which becomes more pronounced when the sheet is larger. In particular and in analogy to single polymers [1], the relevant time scale on which sub-diffusion is observed is given by the rotational relaxation time of the sheet. This time increases with the size of the sheet and thereby enhances the sub-diffusive regime.

Recent Monte Carlo simulations for tethered membranes also reported multi-scale mode dynamics where the center node of the membrane undergoes various sub-diffusive regimes before it enters normal diffusive behavior [11,12]. In our simulations with hydrodynamic interactions included, we observe a much simpler dynamics with just one sub-diffusive regime very similar to polymer dynamics. However, the reported Monte Carlo simulations used much larger sheets compared to our studies. As we just discussed, larger sheets have a smaller diffusion constant and the range of sub-diffusive behavior increases. Since in our simulations we explicitly resolve hydrodynamic interactions, they are highly time consuming. Therefore, we cannot study sheets as large as in refs. [11,12].

3.2 Intermediate scattering function

A widely used quantity to characterize the dynamics of a tethered membrane on different lenght scales is the intermediate scattering function,

$$F(\mathbf{q},t) = \frac{1}{N^2}\sum_{i,j}^{N}\langle \exp(i\mathbf{q}\cdot[\mathbf{r}_i(t)-\mathbf{r}_j(0)])\rangle, \qquad (11)$$

where the wave vector $\mathbf{q}$ sets the length scale of interest. For example, to probe the internal dynamics of a sheet, the wavelength $2\pi/q$ should be much smaller than its linear dimension L. In the following, we investigate the intermediate scattering function to further explore the sub-diffusive behavior of our sheets.

A wave vector $\mathbf{q}$ perpendicular to the plane of the sheet probes the average height fluctuations $\langle[h(t)-h(0)]^2\rangle$. They are related to the size of the sheet by the scaling

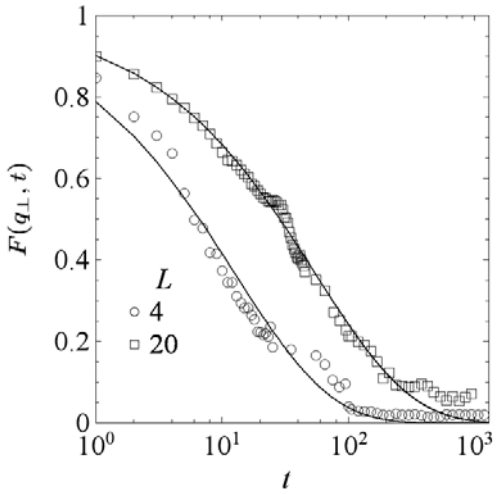

Fig. 7. The intermediate scattering function is plotted as a function of time for $q_\perp = 2\pi$ for sheets with edge length as indicated in the figure. The solid line is given by eq. (12) with $\alpha = 0.57$.

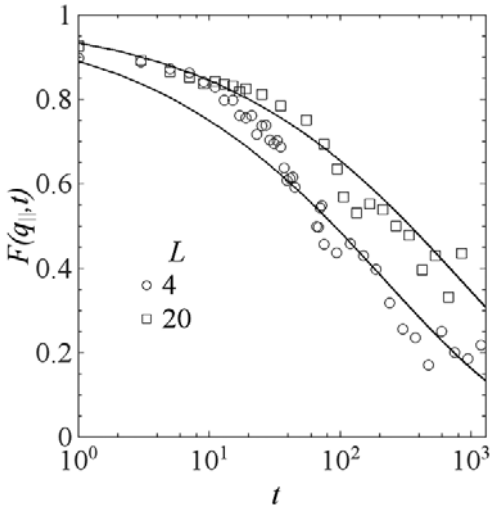

Fig. 8. The intermediate scattering function is plotted as a function of time for $q_\parallel = 2\pi$ for sheets with edge length as indicated in the figure. The solid line is given by eq. (13).

relation $\langle [h(t) - h(0)]^2 \rangle \sim L^\zeta$, where ζ is the roughness exponent. For tethered menbranes, it was calculated in earlier simulation work and found to be in the range 0.5–0.67 [8,28,29]. The sub-diffusive motion of a tethered sheet reported in fig. 6 leads to a stretched exponential in the intermediate scattering function [9]

$$F(q_\perp, t) \sim \exp(-Cq_\perp^2 t^\alpha), \tag{12}$$

where $q_\perp$ is the wave number or magnitude of a wave vector $\mathbf{q}$ perpendicular to the sheet. The exponent α is related to the hight fluctuations of the sheet through the roughness exponent ζ, where α differs for Rouse and Zimm dynamics as calculated in ref. [9] for a tethered membrane. In particular, Zimm dynamics gives $\alpha = 2\zeta/(1+2\zeta)$. In fig. 7 we plot the intermediate scattering function for $q_\perp = 2\pi$ such that $q_\perp L \gg 1$. The solid line is the stretched exponential of eq. (12) with $\alpha = 0.57$. Variations of α beyond ± 0.01 lead to clear deviations from the simulation results. With $\alpha = 0.57$, we calculate the roughness exponent to be $\zeta \approx 0.66$ consistent with earlier work [28,29].

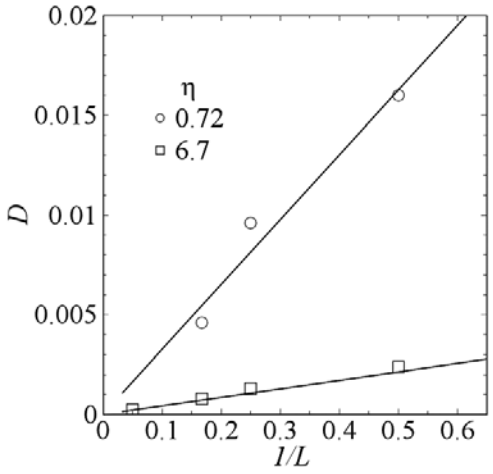

Fig. 9. The diffusion coefficient is plotted as a function of the inverse sheet size L for 2 different viscosities as indicated in the figure. The solid line is given by eq. (14) with $c = 0.025$.

In-plane fluctuations of the sheet scale like L^ω, where ω is the relevant exponent. The intermediate scattering function probes these fluctuations with a wave vector $\mathbf{q}$ parallel to the sheet, where $q_\parallel$ denotes its wave number. For $q_\parallel L \gg 1$, the intermediate scattering function again gives a stretched exponential [9]

$$F(q_\parallel, t) \sim \exp(-Cq_\parallel^2 t^\beta), \tag{13}$$

with $\beta = \omega/(1+\omega)$ [9]. Early analytical calculations determined $\omega = 2/3$ [30], which gives $\beta = 0.4$. In fig. 8 we plot the intermediate scattering function for $q_\parallel = 2\pi$ and use $\beta = 0.4$ in the stretched exponential of eq. (13) which gives a good fit with our numerical results for a sheet size $L = 20$. Deviations occur, however, for the smaller sheet with $L = 4$ due to finite size effects.

3.3 Diffusive regime

In fig. 9 we plot the diffusion coefficient $D = \langle R^2 \rangle / 6t$ as a function of the inverse sheet size L for 2 different viscosities ($\eta = 6.7$ and 0.72). The diffusion coefficient of a flat disc, $D = \frac{2}{3} D_\perp + \frac{1}{3} D_{||}$, where $D_\perp$ and $D_{||}$ describe the respective diffusion parallel and perpendicular to the disc normal, has analytically been calculated in refs. [9,10]. The diffusion coefficient goes as the inverse diameter of the disc

$$D = ck_BT/(\eta L), \tag{14}$$

and $c \sim 0.2$ is a constant whose exact value depends on the approximations used. Our simulations in fig. 9 confirm the $1/L$ scaling. However, the prefactor $c = 0.025$ is smaller by a factor of eight than the value determined for the flat circular disc. A possible reason for the discrepancy are the height fluctuations in our semi-flexible sheet

that increase its two friction coeffcients compared to the infinitely thin rigid sheet treated in refs. [9,10]. The Einstein relation then gives a smaller diffusion coefficient D. A further possible reason might be the quadratic shape of the sheet compared to the circular disc of refs. [9,10]. At least, the area of a quadratic sheet with edge length L is by a factor of 1.27 larger than a ciruclar disc with diameter L which also increases the resistance.

4 Conclusion

In this paper we demonstrated that the method of stochastic rotation dynamics is able to simulate the dynamic properties of a two-dimensional semi-flexible sheet. Since the main contribution to viscosity of the SRD fluid comes from the collision step, we could treat large sheets as penetrable during the streaming step which speeded up our simulations considerably. We identified a sub-diffusive and diffusive regime in the mean-square displacement of the sheet similar to linear polymers. The exponent γ of the sub-diffusive regime was larger compared to simulations without hydrodynamic interactions [12]. The same behavior is also observed for polymers treated in the Rouse and Zimm model. The sub-diffusive behavior is also visible in the intermediate scattering function as stretched exponential, which we reproduced in our simulations. Thereby, we confirmed a prediction between the roughness exponent and the exponent α [9]. Finally, we demonstrated the diffusion coefficient of the sheet to be inversely proportional to the sheet size similar to predictions for a circular disc [9,10].

In recent experiments the self-assembly of DNA-coated polystyrene beads into 2D colloidal crystals was observed that floated above a DNA covered substrate [31]. The structure was called "flying colloidal carpets". This system should show similar dynamic behavior as the sheets studied in this article provided one is able to detach the colloidal carpet from the surface. Furthermore, it will be interesting to increase the number of sheets in our simulations and to study how excluded-volume and hydrodynamic interactions between the sheets influence their inherent sub-diffusive behavior. Finally, our simulated sheet can easily be modified to model muscular thin film swimmers which have only recently been realized experimentally [32].

We like to thank R. G. Winkler, R. B. Pandey, and Madhan Rao for helpful discussions. This work has been supported by DFG under grants STA 352/7-2 and STA 352/9-1.

References

1. M. Doi, S.F. Edwards, *The Theory of Polymer Dynamics* (Clarendon Press, Oxford, 1994).
2. P.E. Rouse, J. Chem. Phys. **21**, 1272 (1953).
3. B.H. Zimm, J. Chem. Phys. **24**, 269 (1956).
4. M.J. Bowick, A. Travesset, Phys. Rep. **344**, 255 (2001).
5. C.F. Schmidt, K. Svoboda, N. Lei, I.B. Petsche, L.E. Berman, C.R. Safinya, G.S. Grest, Science **259**, 952 (1993).
6. M.S. Spector, E. Naranjo, S. Chiruvolu, J.A. Zasadzinski, Phys. Rev. Lett. **73**, 2867 (1994).
7. Y. Kantor, M. Kardar, D.R. Nelson, Phys. Rev. A **35**, 3056 (1987).
8. Y. Kantor, D.R. Nelson, Phys. Rev. A **36**, 4020 (1987).
9. E. Frey, D.R. Nelson, J. Phys. I **1**, 1715 (1991).
10. J. van Vliet, J. Phys. II **4**, 1737 (1994).
11. R.B. Pandey, K.L. Anderson, B.L. Farmer, Phys. Rev. E **75**, 061913 (2007).
12. H. Popova, A. Milchev, Phys. Rev. E **77**, 041906 (2008).
13. H. Popova, A. Milchev, J. Chem. Phys. **127**, 194903 (2007).
14. E. Gauger, H. Stark, Phys. Rev. E **74**, 021907 (2006).
15. A. Malevanets, R. Kapral, J. Chem. Phys. **110**, 8605 (1999).
16. A. Malevanets, R. Kapral, J. Chem. Phys. **112**, 7260 (2000).
17. G. Gompper, T. Ihle, D.M. Kroll, R.G. Winkler, Adv. Polym. Sci. **221**, 1 (2009).
18. A. Malevanets, J.M. Yeomans, Europhys. Lett. **52**, 231 (2000).
19. J.T. Padding, A.A. Louis, Phys. Rev. E **77**, 011402 (2008).
20. Y. Yang, J. Elgeti, G. Gompper, Phys. Rev. E **78**, 061903 (2008).
21. M.T. Downton, H. Stark, J. Phys.: Condens. Matter **21**, 204101 (2009).
22. S.T. Knauert, J.F. Douglas, F.W. Starr, Macromolecules **43**, 3438 (2010).
23. M.P. Allen, D.J. Tildesley, *Computer Simulation of Liquids* (Clarendon Press, Oxford, 1991).
24. Y. Inoue, Y. Chen, H. Ohashi, J. Stat. Phys. **107**, 85 (2002).
25. H. Noguchi, G. Gompper, Phys. Rev. E **72**, 011901 (2005).
26. T. Ihle, D.M. Kroll, Phys. Rev. E **63**, 020201 (2001).
27. T. Ihle, D.M. Kroll, Phys. Rev. E **67**, 066705 (2003).
28. F.F. Abraham, D.R. Nelson, Science **249**, 393 (1990).
29. F.F. Abraham, D.R. Nelson, J. Phys. **51**, 2653 (1990).
30. E. Guitter, F. David, S. Leibler, L. Peliti, J. Phys. **50**, 1787 (1989).
31. N. Geerts, E. Eiser, Soft Matter **6**, 664 (2010).
32. A.W. Feinberg, A. Feigel, S.S. Shevkoplyas, S. Sheehy, G.M. Whitesides, K.K. Parker, Science **317**, 1366 (2007).